Dose Reduction Achieved by Dynamically Collimating the Redundant Rays in Fan-beam and Cone-beam CT

Yan Xia, *Student Member, IEEE*, Martin Berger, Christian Riess, Joachim Hornegger, *Member, IEEE*, and Andreas Maier, *Member, IEEE*

***Abstract*—In X-ray computed tomography (CT), short-scan acquisition that acquires data only over a range of π plus the fan angle, rather than a full range of 2π, is commonly used in circular fan-beam and cone-beam geometry. Such scan aims to reduce acquisition time and radiation dose during data acquisition. However, during a partial circle scan some data are measured once, while other measurements are observed twice. Traditionally, the redundant data are weighted by a smooth function (e.g. the Parker weights) before filtering. In this paper, we present an algorithmic setup that employs dynamic collimation to shield the redundant rays and propose two algorithms to correct the resulting truncation. This approach is able to potentially decrease the dose of 10% for a C-arm CT with fan angle of 10° and of 23% for a diagnostic CT with fan angle of 50°. Evaluation shows that the reconstruction results are of comparable accuracy to the one from standard short-scan FDK, with less dose to the patient.**

***Index Terms*—X-ray Computed Tomography, Dose Reduction, Data Redundancy, Short-scan**

I. Introduction

In X-ray CT, fan-beam data from projections acquired over a range of π plus the fan angle is sufficient for reconstruction. Such a projection interval is referred to as short-scan and is widely used to reduce acquisition time and radiation dose. However, a short-scan measures data once in some views while twice in other views. There are many practical reconstruction algorithms that employ a weighting scheme (e.g., Parker weights [1]) to approximately compensate for the data redundancy in a short-scan. In this paper, we investigated the possibility to block redundant rays during the short scan acquisition by successively moving the collimator into the ray path at the beginning or end of the scan. By doing so, the smooth weighting function can be avoided and the potential dose reduction of up to 23% can be achieved. Furthermore, we propose two truncation correction algorithms to correct the resulting truncation caused by such data acquisition. This approach is able to potentially decrease the dose in a short-scan while retaining good image quality.

Y. Xia, M. Berger, C. Riess, J. Hornegger and A. Maier are with the Pattern Recognition Lab, Friedrich-Alexander-University Erlangen-Nuremberg, 91058 Erlangen, Germany. Y. Xia and J. Hornegger are also with the Erlangen Graduate School in Advanced Optical Technologies (SAOT), Friedrich-Alexander-University Erlangen-Nuremberg, 91052 Erlangen, Germany. (e-mail: yan.xia@cs.fau.de; martin.berger@cs.fau.de; christian.riess@cs.fau.de; joachim.hornegger@cs.fau.de; andreas.maier@cs.fau.de).

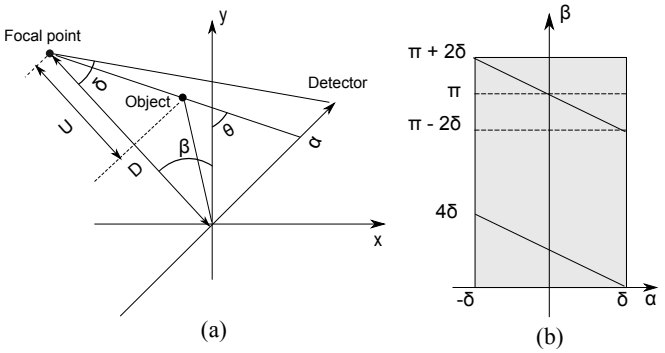

Fig. 1: (a) fan-beam imaging geometry, (b) short-scan sinogram. Notations: β is the rotation angle, α is the relative angular position of an individual ray, δ is half of the fan-beam angle, D is source-detector distance and $\boldsymbol{\theta} = (\cos\theta, \sin\theta)$.

II. Methods

A. Fan-beam Short-scan

Parallel-beam projection data from an angular range of π is sufficient to reconstruct an object. A direct substitution of the integral variables from the parallel-beam data to the fan-beam data leads to the corresponding fan-beam geometry algorithm (see Fig. 1a for the notation):

$$f(\mathbf{x}) = \int_{-\alpha}^{\pi-\alpha} \int_{-\pi/2}^{\pi/2} g(\beta,\alpha)\, h_R(\mathbf{x}\cdot\boldsymbol{\theta} - D\sin\alpha)\, D\cos\alpha \,\mathrm{d}\alpha\mathrm{d}\beta. \tag{1}$$

where $g(\beta,\alpha)$ is the line integral along the ray specified by (β,α), $h_R(\cdot)$ is the Ram-Lak filter kernel and $\mathbf{x} = (x, y)$.

However, Eqn. (1) can not be solved as filtered backprojection since the integration over β depends on the fan angle α. A solution is to extend the projection interval to an angle span of $\pi + 2\delta$, so that integration over β becomes independent of α:

$$f(\mathbf{x}) = \int_{0}^{\pi+2\delta} \int_{-\pi/2}^{\pi/2} \widetilde{g}(\beta,\alpha)\, h_R(\mathbf{x}\cdot\boldsymbol{\theta} - D\sin\alpha)\, D\cos\alpha \,\mathrm{d}\alpha\mathrm{d}\beta, \tag{2}$$

where $\widetilde{g}(\beta,\alpha) = \omega(\beta,\alpha)\, g(\beta,\alpha)$. This projection interval is well-known as short-scan acquisition in contrast to full-scan that covers an angular range of 2π. It is noted that an appropriate weighting function $\omega(\beta,\alpha)$ is applied here since

a short-scan measures some redundant rays at the beginning and at the end of data acquisition (see the two dark triangles in Fig. 1b). In these regions, the relation

$$g(\beta,\alpha) = g(\beta+\pi+2\alpha,-\alpha) \tag{3}$$

holds. The commonly used weighting function for $\omega(\beta,\alpha)$ is the Parker weight [1], in which the projection rays measured twice are normalized to unity while guaranteeing smooth transitions between non-redundant and redundant data.

B. Dynamic Collimation

In X-ray imaging, the collimator is typically deployed to statically shield the unnecessary radiation outside a specified region of interest (ROI). In this work, we investigate the possibility to block redundant rays during short-scan acquisition by successively moving the collimator into the ray path at the beginning or end of the scan. Fig. 2 illustrates the potential dose irradiated to the patient (red color) in such data acquisition compared to a traditional short-scan. The resulting dose reduction can be theoretically estimated as the ratio between the short scan area A_s and the collimated redundant area A_r (see Fig. 1b)

$$R = \frac{A_r}{A_s} = \frac{\frac{1}{2}2\delta\cdot 4\delta}{2\delta(\pi+2\delta)} = \frac{2\delta}{\pi+2\delta}. \tag{4}$$

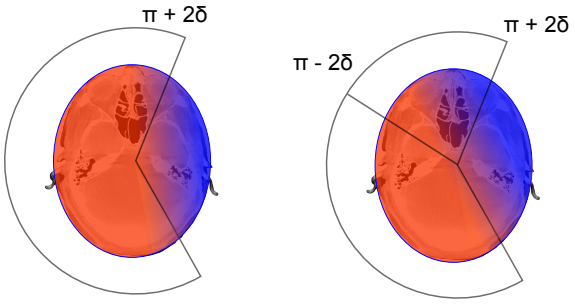

Fig. 2: Illustration of the dose irradiated to the patient for a traditional short-scan (left) and for the proposed scan (right). The red color indicates the dose exposure to the patient.

Using such a dynamic collimation for the redundant data is equivalent to applying a binary weighting function as follows

$$\omega_{\mathrm{b}}(\beta,\alpha) = \begin{cases} 1 & \text{if} \quad 0 \leqslant \beta \leqslant \pi+2\alpha, \\ 0 & \text{otherwise.} \end{cases} \tag{5}$$

This binary weight ensures that Eqn. (1) and (2) are mathematically identical but introduces high frequencies at the borders of the non-redundant area. Thus, after filtering and backprojection, severe streaking artifacts will be observed in the reconstruction. To tackle this shortcoming, two truncation correction methods are introduced in the following sections. Note that both algorithms are computationally very efficient and thus do not affect reconstruction speed.

C. Water Cylinder Extrapolation

A widely-used approach to model missing data is extrapolation with a partial cylindrical water object. If only one side of the projection data is truncated, then the extended projection data $\widetilde{g}_{\text{ext}}(\beta,\alpha)$ is computed by

$$\widetilde{g}_{\text{ext}}(\beta,\alpha) = \begin{cases} \widetilde{g}(\beta,\alpha) & \text{if} \quad 0 \leqslant \beta \leqslant \pi+2\alpha, \\ 2\mu_w\sqrt{x^2(\beta)+r^2(\beta)} & \text{otherwise.} \end{cases} \tag{6}$$

where $\mu_w = 0.025$ denotes the attenuation coefficient of water. The choice of the location $x(\beta)$ and the radius $r(\beta)$ of the fitted water cylinder are represented in Ref. [2]. Since we extrapolate the redundant area which is supposed to be 0, a constant weight needs to be applied to this area after the filtering; see the full paper for the implementation details.

D. ATRACT

As an alternative, we consider a recent approach for truncation correction named the approximated truncation robust algorithm for computed tomography (ATRACT). It is able to reconstruct the truncated data without explicit extrapolation. The idea of ATRACT is to decompose the Ram-Lak filter into a purely local Laplacian and a residual filtering kernel that is less sensitive to data truncation. In this work we use the 1D version of ATRACT [3] and the algorithm in fan-beam geometry can be derived as follows.

First, we define the new variable D' and α', with $\mathbf{x}\cdot\boldsymbol{\theta} - D\sin\alpha = D'\sin(\alpha'-\alpha)$. Then, Eqn. (2) can be rewritten as:

$$f(\mathbf{x}) = \int_0^{\pi+2\delta}\int_{-\pi/2}^{\pi/2} \widetilde{g}(\beta,\alpha)\, h_R(D'\sin(\alpha'-\alpha))\, D\cos\alpha\,\mathrm{d}\alpha\mathrm{d}\beta. \tag{7}$$

Note that the Ram-Lak filter $h_R(\cdot)$ can be further decomposed into a Laplace operator and a residual global filter with a kernel $\ln(\cdot)$:

$$f(\mathbf{x}) = \int_0^{\pi+2\delta} \frac{1}{2\pi^2 D'} \int_{-\pi/2}^{\pi/2} \frac{1}{D\cos\alpha}\frac{\partial^2}{\partial\alpha^2}\widetilde{g}(\beta,\alpha) \ln\left|\tan\left((\alpha'-\alpha)/2\right)\right| D\cos\alpha\,\mathrm{d}\alpha\mathrm{d}\beta, \tag{8}$$

where D' is the distance from the reconstruction point to the source at the angle β. By introducing a proper intermediate function, the factor D' can be eliminated as follows:

$$g_F(\beta,\alpha') = \int_{-\pi/2}^{\pi/2} \frac{\partial^2}{\partial\alpha^2}\widetilde{g}(\beta,\alpha)\ln\left|\tan\left((\alpha'-\alpha)/2\right)\right|\mathrm{d}\alpha, \tag{9}$$

$$f(\mathbf{x}) = \frac{1}{2\pi^2 D}\int_0^{\pi+2\delta}\frac{1}{\cos\alpha'} g_F(\beta,\alpha')\,\mathrm{d}\beta. \tag{10}$$

The equations above can be adapted for a flat-panel detector

	Phantom	Real Data
scan radius	800 mm	750 mm
scan interval $\pi + 2\delta$	200°	200°
angular increment $\triangle\beta$	1.5°	0.4°
detector-source distance D	1000 mm	1196 mm
detector pixel size	0.65 mm	0.308 mm
detector area	300×400 mm^2	300×400 mm^2

Table I: Geometrical parameters of the simulated phantoms and real data.

by introducing $t = D \sin\alpha$:

$$f_{\text{flat}}(\mathbf{x}) = \frac{1}{2\pi^2} \int_0^{\pi+2\delta} \frac{1}{U^2} \int_{-\infty}^{\infty} \frac{\partial^2}{\partial t^2} \left[\frac{D}{\sqrt{D^2+t^2}} \widetilde{g}(\beta, t) \right] \ln|t' - t| \, \mathrm{d}t \mathrm{d}\beta. \quad (11)$$

So far we only present the ATRACT algorithm in the fan-beam geometry. However, it was also shown in Ref. [3] that these equations can be readily extended to a cone-beam geometry.

III. Experiments and Results

Both, simulated phantom and real data (courtesy of St. Lukes' Episcopal Hospital, Houston, TX, USA) have been involved in the validation of the proposed methods. The configuration parameters can be found in Table I. The simulated data were generated using the Siemens X-ray simulation Software DRASIM with a pre-defined FORBILD head phantom[1]. The real clinical data were acquired on a C-arm CT system with 496 projections (1240×960 px) at the resolution of 0.308 mm/ px.

Two experimental configurations were considered. In configuration 1, no collimation was applied, yielding the non-truncated short-scan data. In the second one, the datasets were virtually cropped so that only non-redundant data were kept. All reconstructions were carried out into a volume of $512 \times 512 \times 350$ with an isotropic voxel size of $0.45\,\text{mm}^3$. The standard FDK reconstruction of configuration 1, i.e. short scan non-truncated data were used as reference in each case. The truncated datasets from proposed data acquisition were reconstructed by the ATRACT and FDK algorithm, referring as binary-weighted ATRACT and binary-weighted FDK in the following.

A. Dose Reduction

Fig. 3 depicts the possible dose reduction for short-scan acquisition in C-arm CT and diagnostic CT according to the theoretical estimation using Eqn. (4). We can see that the amount of reduction is proportional to the fan-beam angle, e.g., for a diagnostic CT with a large fan-beam angle of 50° dose reduction of up to 23% is reached.

[1]http://www.imp.uni-erlangen.de/forbild

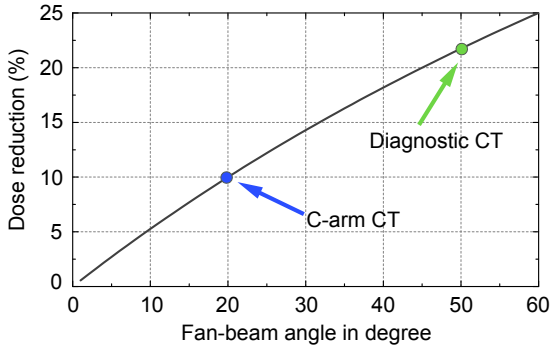

Fig. 3: Dose reduction as a function of the fan angle 2δ.

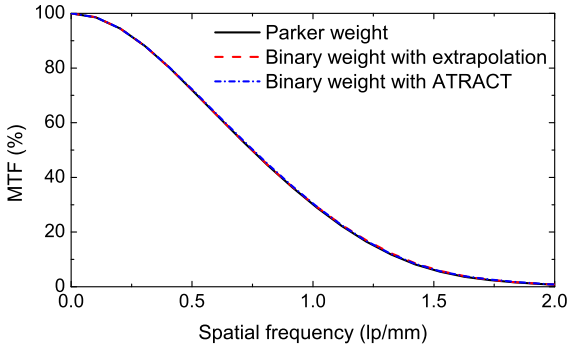

Fig. 4: MTFs for the central bead (diameter: 0.25 mm).

B. Spatial Resolution

Reconstruction resolution from Parker-weighted FDK, binary-weigthed extrapolation method as well as binary-weighted ATRACT was matched by computing the modulation transfer function (MTF) using a simulated bead phantom, as shown in Fig. 4.

C. Streaking Artifacts Suppression

We used a 3D noise-free FORBILD head phantom to analyze the image quality of the proposed methods and compared it to that of standard Parker-weighted FDK (see Fig. 5). It is clear that the straightforward FDK method can not handle the data truncation introduced by the proposed scan acquisition: streaking-like artifacts are obviously observed in the reconstruction that are oriented to a certain direction. On the other hand, both binary-weighted extrapolation and ATRACT are able to significantly eliminate the streaks and yield the comparable image quality to the reference.

D. Noise Estimation

The same FORBILD head phantom is applied with artificially added noise. The noise level is estimated by computing the standard deviation in selected ROIs (marked in Fig. 5) and represented in Table II. Reconstructed results are shown in Fig. 6. From Table II we can see that no significant differences are observed among all three algorithms in terms of noise estimation, confirming that the proposed data acquisition is able to achieve dose reduction without increasing the noise in the images.

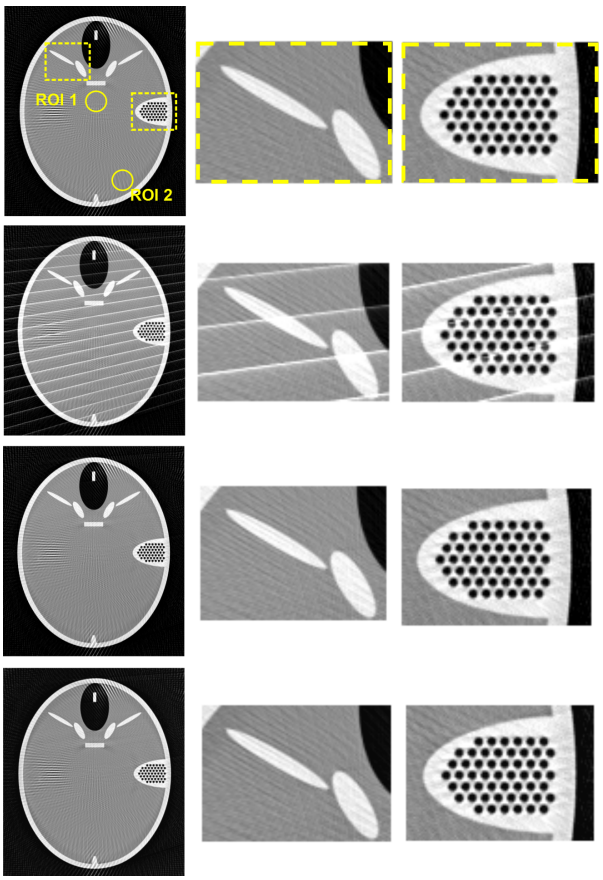

Fig. 5: Reconstructed slices ($z = 0\,\text{mm}$) of the noise-free FORBILD phantom ($C = 0\,\text{HU}, W = 2000\,\text{HU}$). From top to bottom: Parker-weighted FDK, binary-weighted FDK, binary-weighted extrapolation and ATRACT.

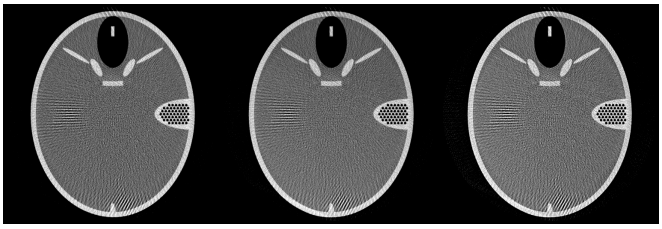

Fig. 6: Reconstructed slices ($z = 0\,\text{mm}$) of the noise FORBILD phantom ($C = 200\,\text{HU}, W = 1600\,\text{HU}$). From left to right: Parker-weighted FDK, binary-weighted extrapolation and ATRACT.

E. Real Data Evaluation

Reconstructed results from real clinical data using the binary-weighted ATRACT and Parker-weighted FDK algorithm are shown in Fig. 7. Again, no substantial differences are observed in the transversal and sagittal planes of the reconstruction from parker-weighted FDK and binary-weighted ATRACT.

	Parker weight	Extrapolation	ATRACT
ROI 1	170.90	172.77	168.32
ROI 2	174.48	175.46	169.00

Table II: Noise estimation by computing the standard deviation (HU) in two ROIs for the noise FORBILD phantom reconstructions.

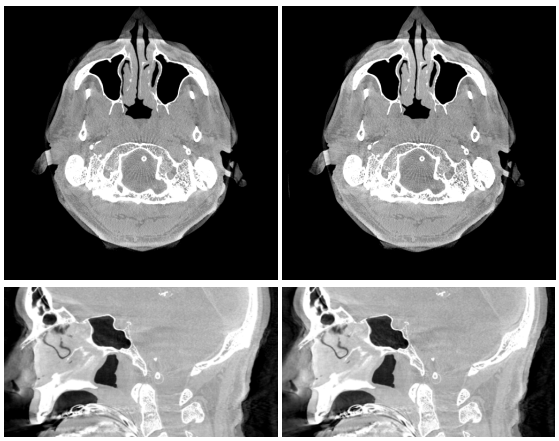

Fig. 7: Transversal slice ($z = 0\,\text{mm}$) and sagittal slice ($x = 0\,\text{mm}$) of the reconstructions from clinical data ($C = 0\,\text{HU}, W = 500\,\text{HU}$). From left to right: Parker-weighted FDK, binary-weighted ATRACT.

IV. Conclusion

We presented in this paper an algorithmic setup that is able to further reduce the radiation dose to the patient in a short-scan data acquisition. The evaluation showed that our proposed approach achieved image quality similar to that of Parker-weighted short-scan FDK with less dose potentially irradiated to the patient. We expect that the new approach could be combined with so-called super short-scan suggested in [4] and [5]. When only a small ROI is required to be reconstructed in the object, the angular interval of short-scan can be further relaxed to less than π plus the fan angle, i.e, super short-scan. The combination of removal of redundant data and shorter acquisition trajectory will result in dose-minimized complete data for reconstruction.

Acknowledgment

The authors gratefully acknowledge funding by Siemens AG, Healthcare Sector and of the Erlangen Graduate School in Advanced Optical Technologies (SAOT) by the German Research Foundation (DFG) in the framework of the German excellence initiative. The authors also would like to thank Dr. Mawad in St. Luke's Episcopal Hospital for providing the valuable clinical data sets. All reconstruction results were computed with a Siemens prototype software, not a clinical product. The concepts and information presented in this paper are based on research and are not commercially available.

References

[1] D. L. Parker, "Optimal short scan convolution reconstruction for fan-beam CT," *Med. Phys.*, vol. 9, pp. 254–257, 1982.

[2] J. Hsieh, E. Chao, J. Thibault, B. Grekowicz, A. Horst, S. McOlash, and T. J. Myers, "A novel reconstruction algorithm to extend the CT scan field-of-view," *Med. Phys.*, vol. 31, pp. 2385–2391, 2004.

[3] Y. Xia, A. Maier, F. Dennerlein, H. Hofmann, K. Mueller, and J. Hornegger, "Reconstruction from truncated projections in cone-beam CT using an efficient 1D filtering," in *Proc. SPIE*, 2013, p. 86681C.

[4] F. Noo, M. Defrise, R. Clackdoyle, and H. Kudo, "Image reconstruction from fan-beam projections on less than a short scan," *Phys. Med. Biol.*, vol. 47, pp. 2525–2546, 2002.

[5] H. Kudo, F. Noo, M. Defrise, and R. Clackdoyle, "New super-short-scan algorithms for fan-beam and cone-beam reconstruction," in *Nuclear Science Symposium Conference Record*, vol. 2, 2002, pp. 902–906.